Oxygen exchange kinetics on solid oxide fuel cell cathode materials—general trends and their mechanistic interpretation

Lei Wang[a] and Rotraut Merkle[b]
Max Planck Institute for Solid State Research, 70569 Stuttgart, Germany

Yuri A. Mastrikov[c]
Max Planck Institute for Solid State Research, 70569 Stuttgart, Germany; and University of Maryland, College Park, Maryland 20742-2115

Eugene A. Kotomin and Joachim Maier
Max Planck Institute for Solid State Research, 70569 Stuttgart, Germany

(Received 19 January 2012; accepted 21 May 2012)

The compilation of measured effective rate constants for oxygen surface exchange on mixed conducting perovskites, which covers a great variety of compositions ranging from (La,Sr)$MnO_{3-\delta}$ to (La,Sr)(Co,Fe)$O_{3-\delta}$ and (Ba,Sr)(Co,Fe)$O_{3-\delta}$, demonstrates the importance of ionic conductivity—i.e., high oxygen vacancy concentration as well as vacancy mobility—as a key factor for the surface oxygen exchange rate. This interpretation is corroborated by ab initio calculations, which indicate that the approach of an oxygen vacancy to oxygen intermediates adsorbed on the surface is the rate determining step for a number of perovskites.

I. INTRODUCTION

The exchange reaction of oxygen between gas phase and solid is of interest from a fundamental point of view elucidating the mechanism of one of the "simplest" gas–solid reactions, as well as for its importance for electrochemical devices such as solid oxide fuel cells (SOFC), permeation membranes, and electrochemical sensors, which rely on a fast oxygen incorporation reaction.

It is not the goal of this article to analyze the rates of oxygen exchange in greatest detail. Rather, we want to extract key properties of major influence on oxygen exchange kinetics for a large range of materials. Naturally, such correlations are only sensible for comparable reaction mechanisms and most straightforward if the rate determining step (*rds*) remains the same (if mass action constants representing the quasiequilibrated fast reactions before and after the *rds* are also affected by changes of the properties governing the *rds*, this may lead to deviations from the idealized correlation). As discussed below, this condition is fulfilled for a large range of oxygen-deficient mixed conducting perovskites (and may even apply to perovskite-related materials such as A-site ordered double perovskites, as long as oxygen vacancies $V_O^{\cdot\cdot}$ determine oxygen transport). For materials of different structure type (and/or oxygen exchange being confined to the reaction at the surface with immediate desorption, i.e., not including oxygen incorporation into $V_O^{\cdot\cdot}$), different relations are expected.

We will not deal with materials where the B site is mainly occupied by redox-inactive cations such as Ti in slightly Fe-doped $SrTiO_3$ or the $SrTi_{1-x}Fe_xO_{3-\delta}$ solid solution series with low Fe content. For those "electron-poor" materials, indeed, the limited availability of electronic charge carriers can become the main limiting factor.[1–3] Instead, we will focus on (Ba,Sr,La)(Mn,Fe,Co)$O_{3-\delta}$ perovskites.

As a basis for the discussion, we use oxygen exchange experiments on dense bulk samples (isotope exchange and conductivity relaxation) as well as on pore-free films deposited by pulsed laser deposition (PLD) on Y-stabilized ZrO_2 (YSZ) substrates (electrochemical O exchange measured by impedance spectroscopy). Owing to the varying morphology and thus surface area (which is usually not quantified, apart from few focused ion beam scanning electron microscopy investigations, see e.g., Refs. 4 and 5), results from porous films (or even porous composite films) cannot be used in this discussion, which aims at comparing the intrinsic materials properties. For this reason, we will also exclude extremely thin films from the discussion, although their often accelerated oxygen exchange may be related to increased concentration and/or mobility of vacancies (see e.g., Ref. 6).

Since the oxygen incorporation surface reaction exhibits a complex network of possible reaction pathways in which the *rds* has to be identified, the analysis requires the measurement of effective rate constants, together with in situ surface analytical investigations as far as available

[a]Present address: Massachusetts Institute of Technology, Cambridge, MA
[b]Address all correspondence to this author.
e-mail: r.merkle@fkf.mpg.de
[c]Present address: Institute for Solid State Physics, University of Latvia, Riga, Latvia
DOI: 10.1557/jmr.2012.186

 © Materials Research Society 2012

https://doi.org/10.1557/jmr.2012.186 Published online by Cambridge University Press

(not discussed in this paper), a phenomenological kinetic description, and ab initio studies.

II. EXPERIMENTAL

Polycrystalline, dense (La,Sr)$MnO_{3-\delta}$ (LSM), (La,Sr)(Co,Fe)$O_{3-\delta}$ (LSCF), and (Ba,Sr)(Co,Fe)$O_{3-\delta}$ (BSCF) films were deposited by PLD on YSZ single crystals, typically 100 nm thick. The films were patterned by lithography and ion beam etching into circular "microelectrodes" with 20–100 μm diameter, which are then individually contacted with Pt/Ir tips for electrochemical impedance measurements (see also Refs. 7 and 8). Details for determination of tracer diffusion coefficient D^* in BSCF films are given in Ref. 9. Density functional theory (DFT) calculations for LSM and BSCF were performed with GGA-PW91 and GGA-PBE exchange–correlation functionals as implemented in the VASP code. Transition states for reaction and ion migration were located using the climbing image nudged elastic band method (see also Refs. 10 and 11).

III. RESULTS AND DISCUSSION

A. Empirical relation involving ionic conductivity

The first step in understanding the mechanistic details of a reaction is to identify those species which are important for the *rds* and hence crucial for the overall rate (nevertheless, parameters of fast preceding/succeeding steps can also affect the rate). Thus, in the case of a gas–solid surface reaction, correlations with the nature and concentrations of surface species (e.g., adsorbates) and surface defects (e.g., oxygen vacancies) come to the fore. Unfortunately, in the window of relevant conditions (300–800 °C, $pO_2 \approx 0.2$ bar), the surface defect concentrations are experimentally accessible in the fewest cases. We are aware of the fact that defect energetics and thus absolute concentrations in the surface layer differ from the bulk. Nevertheless, as long as the same reactions determine the equilibration with the gas phase and the majority defects remain the same, the pO_2 dependence of defect concentrations in bulk and surface layer will be similar (this at least holds for an electroneutral model). In addition to the different surface energetics, surface space charge zones may modify the kinetics, e.g., for slightly Fe-doped $SrTiO_3$.[12] In the materials under discussion, however, such space charge zones can be assumed to be negligible (the blocking character of the grain boundaries in $SrTi_{1-x}Fe_xO_{3-d}$ vanishes with increasing Fe content, i.e., increasing carrier density and concentration of cations with variable valence, at ≥7 mol% of Fe[13]).

Figure 1(a) shows effective rate constants k^q of the oxygen surface reaction (determined from impedance measurements of perovskite films on YSZ substrates) versus electronic conductivity. No clear trend can be recognized—for instance, $Ba_{0.5}Sr_{0.5}Co_{0.8}Fe_{0.2}O_{3-\delta}$ with the fastest exchange rate has a lower electronic conductivity

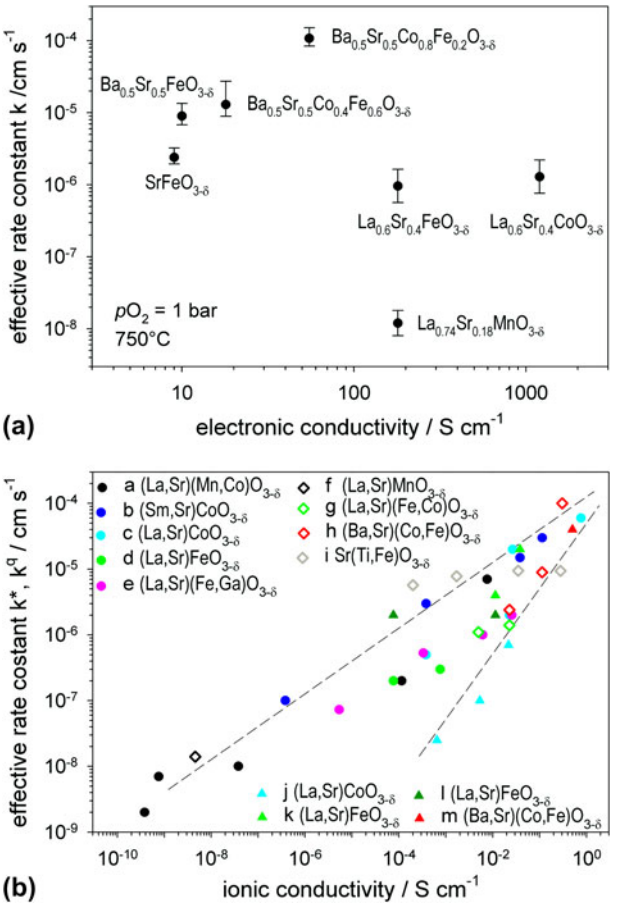


FIG. 1. (a) Effective oxygen exchange rate constants k^q of mixed conducting perovskites at 750 °C and $pO_2 = 1$ bar plotted versus electronic conductivity. k^q from Refs. 7, 8, and 14, σ_{eon} from Refs. 15–19. (b) Rate constants at 750 °C, $pO_2 = 1$ bar for bulk samples [circles: k^*, triangles: $k^* = k^{chem}/w_O$ from chemical relaxation experiments, $w_O = 0.5(\partial \ln pO_2/\partial \ln c_O)$] and dense PLD films (diamonds: k^q) plotted versus ionic conductivity (in most cases calculated from diffusivity via Nernst–Einstein relation). For the interpretation of the dashed lines, see Sec. III. C. Data sources: a,[20] b,[21] c,[22] d,[23] e,[24] f,[14] g,[7] h,[8] i: k^q from,[3] σ_{ion} from,[25] j[26] (with w_O taken from Ref. 27) k,[28] l,[29] m.[30] If necessary, data were interpolated/extrapolated: pO_2 dependences from the references were used where available. Otherwise, D^* which typically has a less pronounced dependence was not adjusted, while k^* was extrapolated to 1 bar with the approximate relation $k^* \propto (pO_2)^{0.5}$, which is reasonably close to many experimentally found exponents.

than $La_{0.74}Sr_{0.18}MnO_{3-\delta}$ with the lowest rate. Although electrons must be involved in the oxygen exchange reaction, obviously, the supply of electronic carriers is not rate limiting for the perovskites considered here.

Figure 1(b) shows effective rate constants k determined by isotope exchange (k^*) as well as k^q (k^* and k^q are related by the same proportionality factor to the exchange rate of the oxygen incorporation reaction $\Re_0$ and thus refer to the same quantity[31]; in some places, we will drop the superscript for simplicity) from electrochemical measurements on pore-free thin films plotted versus bulk ionic conductivity. For a given material, the scatter in the bulk property σ_{ion} is smaller

https://doi.org/10.1557/jmr.2012.186 Published online by Cambridge University Press

compared to the surface rate constant k, which is more sensitive to sample preparation, aging, etc., thus preferably, data from the same source should be used for more detailed comparisons. One clear trend is observed; typically, the samples with a higher ionic conductivity also exhibit a faster surface reaction. The fact that a higher oxygen vacancy concentration typically leads to faster surface exchange has been observed and discussed already in Refs. 20, 28, 29, 32, and 33. Based on results for BSCF perovskites,[8] it was further concluded that not only $V_O^{\cdot\cdot}$ concentration but also $V_O^{\cdot\cdot}$ mobility can significantly affect the surface reaction rate. To understand these correlations, reaction mechanisms for some perovskites will be discussed in more detail in the next section.

The importance of ionic conductivity for SOFC cathode performance is well established as a certain σ_{ion} is required to allow for oxygen incorporation on the whole surface of the cathode material ("bulk path"[34]) instead of being limited to the extremely narrow zone of the three-phase boundary. With its correlation to surface exchange kinetics as discussed here, σ_{ion} must be regarded as even more important since it increases not only the electrocatalytically active part of an electrode layer but also the actual surface reaction rate.

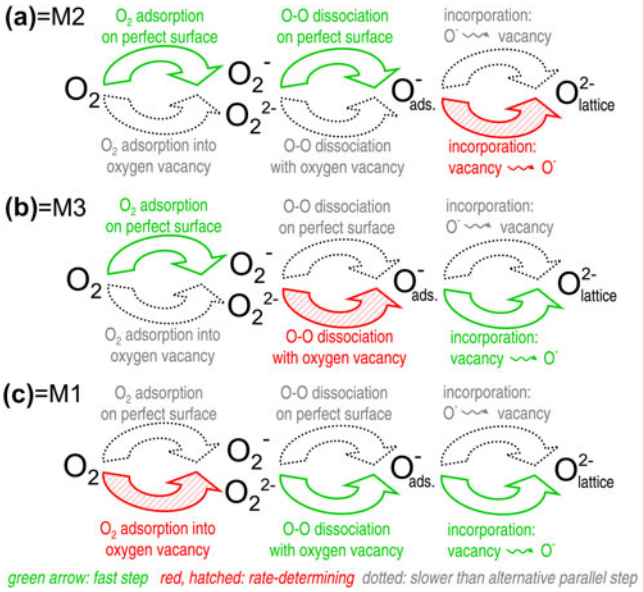


FIG. 2. Schematic network of possible reaction steps for the oxygen incorporation into mixed conducting perovskites. (a) Predominant mechanism for perovskites with very low oxygen vacancy concentration such as LSM, =M2 in Fig. 3; (b) for perovskites with high vacancy concentration such as LSCF or BSCF, =M3 in Fig. 3; (c) hypothetical mechanism starting with adsorption into vacancy, =M1 in Fig. 3.

B. Detailed mechanistic considerations for LSM, LSCF, and BSCF

For LSM (the first perovskite widely applied as SOFC cathode material), extensive ab initio calculations are available, which allow detailed atomistic insight into the reaction mechanism that could not be extracted solely from experiments[10,35] (unfortunately, due to the very small supercell used, the mutual approach of adsorbed oxygen species and $V_O^{\cdot\cdot}$ is not dealt with in Ref. 35). As a first step, the most stable surface terminations need to be identified as they are expected to be the most exposed ones in the actual experiments with typically polycrystalline samples. For $LaMnO_3$, under relevant SOFC conditions (high T, high pO_2), the MnO_2(001) termination is found most stable,[10] while for Sr-doped LSM, the (La,Sr)O(001) termination can become comparably stable or even slightly lower in energy but only at low pO_2.[10,36,37] Nevertheless, the formation of oxygen vacancies $V_O^{\cdot\cdot}$ as an essential ingredient for oxygen incorporation is unfavorable by about 2 eV on (La,Sr)O(001) compared to MnO_2(001). At 1000 K, this corresponds to a decrease in $V_O^{\cdot\cdot}$ concentration by more than 9 orders of magnitude, which will decelerate any mechanism accordingly (directly if the *rds* already contains $V_O^{\cdot\cdot}$; or by making the last step requiring $V_O^{\cdot\cdot}$, see Fig. 2, rate limiting due to their low concentration). Thus, even if the (La,Sr)O(001) termination would cover 99% of the total exposed surface area, its contribution to the overall oxygen exchange rate will be negligible.

Therefore, the further mechanistic discussion (see Ref. 10 for more details) will focus on the MnO_2(001) termination. As basis for exploring the network of possible reaction steps (Fig. 2), energies of defects and intermediate species as well as relevant reaction and migration barriers were calculated for $LaMnO_3$. While the formation of adsorbed oxygen species is exothermic (by −1.1 eV for O_2^-, −0.9 eV for O_2^{2-}, −2.2 eV for 2 O_{ad}^-, relative to $O_{2,gas}$), the negative entropy for the adsorption process and repulsive interaction of charged adsorbates at high coverage[38] restrict the estimated adsorbate coverages to <0.01 for O_2^-, O_2^{2-} and ≤0.1 for O_{ad}^-. Oxygen vacancy formation (according to $O_O^x \leftrightarrow 0.5\,O_2 + V_O^{\cdot\cdot} + 2\,Mn_{Mn}^{'}$) is easier by ≈1 eV in the MnO_2(001) surface layer compared to bulk, corresponding to a much larger $V_O^{\cdot\cdot}$ concentration in the surface layer. The $V_O^{\cdot\cdot}$ migration barrier in the surface layer is lower by 0.3 eV. Dissociation of O_2^{2-} on the perfect surface has a barrier of 0.6 eV, while after insertion of O_2^{2-} into a vacancy, dissociation occurs without barrier. Overall rates for different pathways M1–M3 in the reaction network (Fig. 2) can then be estimated as a function of surface vacancy concentration (obtained from measured bulk D^*[39] and $D_{V_O^{\cdot\cdot}}$[23] values for $La_{0.8}Sr_{0.2}MnO_{3\pm\delta}$, and the decreased formation energy in the surface layer) and coverage with adsorbed O_2^- or O_2^{2-}, as shown in Fig. 3.

Pathway M1 [Fig. 2(c)] starting with oxygen adsorption into a surface vacancy is unfavorable under the relevant conditions due to the low vacancy concentration on the LSM surface (cyan area in Fig. 3). Alternative paths begin

https://doi.org/10.1557/jmr.2012.186 Published online by Cambridge University Press

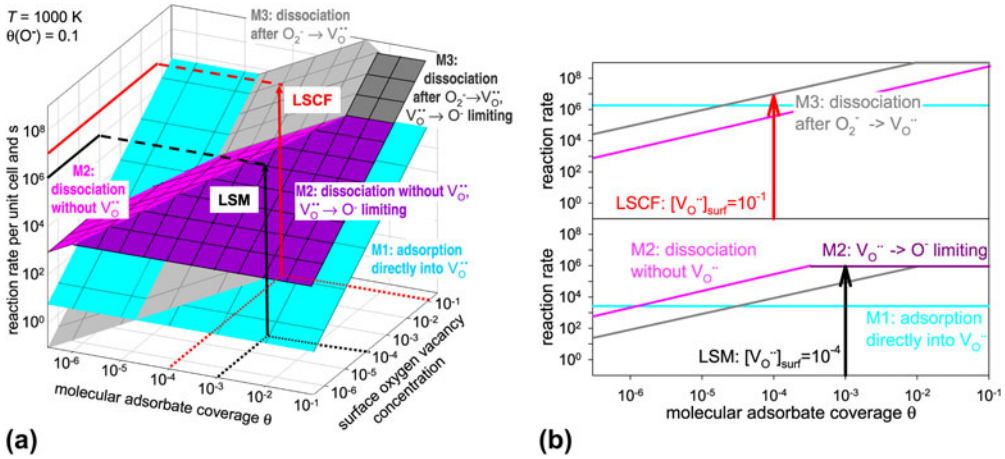


FIG. 3. (a) Reaction rates for three alternative reaction pathways of oxygen incorporation on the MnO_2(001) surface of LSM (black lines) and LSCF (red lines) estimated based on DFT results. Adapted with permission from Ref. 10, copyright (2010) American Chemical Society. (b) Two-dimensional projection for surface vacancy concentration of 10^{-4} (LSM) and 10^{-1} (LSCF).

with adsorption on the perfect surface. Again due to the low $V_{\ddot{O}}$ concentration, the dissociation with assistance of a vacancy [M3, Fig. 2(b)] is unfavorable although the reaction barrier is negligibly small. Thus, path M2 [Fig. 2(a)] with dissociation without $V_{\ddot{O}}$ being involved provides the fastest overall rate. Within this path, either the dissociation is predicted to be rate limiting [at low adsorbate coverage, i.e., very low pO_2, pink area in Fig. 3(a)], or the final incorporation step of O_{ad}^{-} into a surface $V_{\ddot{O}}$ (violet area). Interestingly, the barrier for O_{ad}^{-} migration along the surface is so high (2 eV, due to an unfavorable transition state with the migrating O_{ad}^{-} located atop an oxide ion) that it is the surface vacancy, which approaches O_{ad}^{-} (the actual incorporation then occurs without barrier). For this step being rate determining, the reaction rate is proportional to the product of $V_{\ddot{O}}$ concentration and $V_{\ddot{O}}$ mobility, the latter quantity playing the role of the rate constant (the rate for an individual $V_{\ddot{O}}$ to meet an O_{ad}^{-} is proportional to D/d^2 where d is the mean distance between $V_{\ddot{O}}$ and O_{ad}^{-}, and D is the diffusion coefficient of $V_{\ddot{O}}$ in the surface layer). The proportionality of the rate to the vacancy concentration $[V_{\ddot{O}}]$ is straightforward, as long as preceding equilibria do not involve $[V_{\ddot{O}}]$.

Under the assumption that the reaction and migration barriers do not change drastically, Fig. 3(a) can even be used to "extrapolate" reaction rates to closely related perovskites such as LSCF (the measured bulk vacancy migration barrier around 0.8 eV is similar for LSM and LSCF[23,39]). The vacancy concentration of LSCF is much higher than for LSM as a result of the less negative oxidation enthalpy.[27,40] On the other hand, this also leads to lower adsorbate concentrations since enthalpies of adsorption and oxidation—both involving electron transfer from the transition metal to oxygen—are closely coupled (the calculated energy for molecular oxygen adsorption amounts to ≈1/4 and for two O_{ad}^{-} to ≈1/2 of the O_2 incorporation energy[41]). This is depicted in Fig. 3 by red lines. Owing to the much higher $V_{\ddot{O}}$ concentration for LSCF, path M3 with vacancy-assisted dissociation of O_2^- or O_2^{2-} is predicted to become the most favorable, with the encounter of molecular adsorbed oxygen and $V_{\ddot{O}}$ before the dissociation being rate limiting as shown by the light gray area in Fig. 3(a). The encounter of O_{ad}^{-} and $V_{\ddot{O}}$ for the final incorporation is faster due to the coverage of O_{ad}^{-} being higher than for molecular adsorbate species. The prediction of higher reaction rates for LSCF compared to LSM in Fig. 3 is in agreement with experiments.[7]

The investigation of BSCF perovskites also yields valuable insight into the oxygen exchange reaction mechanism. $Ba_{0.5}Sr_{0.5}Co_{0.8}Fe_{0.2}O_{3-\delta}$ was initially developed for oxygen permeation membranes (i.e., high electronic and ionic conductivity) but then found to exhibit also very fast surface exchange kinetics.[42,43] A plot of k^q (measured by impedance spectroscopy on pore-free films on YSZ) for different cation compositions within the $Ba_{1-x}Sr_xCo_yFe_{1-y}O_{3-\delta}$ family versus $V_{\ddot{O}}$ concentration yields a clear but nonlinear correlation.[8] In contrast to the perovskites of the (La,Sr)(Mn,Fe,Co)$O_{3-\delta}$ family, the mobility of $V_{\ddot{O}}$ increases in BSCF with increasing content of Ba and Co. Only, when plotting k^q versus D^* ($\propto \sigma_{ion}$), an approximately linear correlation is obtained (Fig. 4). For hexagonal $Ba_{0.5}Sr_{0.5}Co_{0.8}Fe_{0.2}O_{3-\delta}$, a lower ionic conductivity than for the cubic phase is expected (based on analogy to the closely related cubic/hexagonal $SrCoO_{3-\delta}$[44]). Interestingly, an investigation of oxygen exchange in $Ba_{0.5}Sr_{0.5}Co_{0.8}Fe_{0.2}O_{3-\delta}$ during its slow transformation to the hexagonal perovskite phase also yields a linear correlation between k^{chem} ($= w_O \cdot k^q$) and D^{chem} ($= w_O \cdot D^*$) (open symbols in Fig. 4).[45] Thus, increasing vacancy concentration and vacancy mobility ($D_{V_{\ddot{O}}}$) enhance the reaction rate. The latter makes the stronger contribution in the series $SrFeO_{3-\delta}$–$Ba_{0.5}Sr_{0.5}FeO_{3-\delta}$–BSCF (increasing by a factor of 18 at 600 °C from SF to BSCF) than the vacancy

https://doi.org/10.1557/jmr.2012.186 Published online by Cambridge University Press

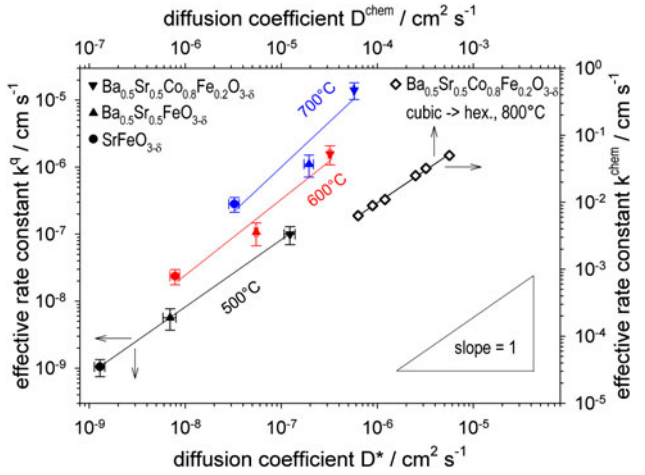


FIG. 4. Effective rate constant for oxygen exchange on BSCF plotted versus diffusion coefficient. Solid symbols: k^q, D^* ($\propto \sigma_{ion}$) from Ref. 8, $pO_2 = 0.2$ bar (k^q), 0.5 bar (D^*). Open symbols: k^{chem} ($=w_O k^q$), D^{chem} ($=w_O D^*$) for a $Ba_{0.5}Sr_{0.5}Co_{0.8}Fe_{0.2}O_{3-\delta}$ sample, which slowly transforms from cubic to a hexagonal perovskite phase from Ref. 45, $pO_2 = 0.33 \leftrightarrow 1$ bar O_2.

concentration, which is already high for $SrFeO_{3-\delta}$ to ($\delta = 0.25$) and increases only moderately for BSCF ($\delta = 0.53$). Pronounced differences in oxygen migration barriers in the BSCF perovskites were found also in ab initio calculations.[11] Geometrical constraints such as the distance of the migrating O to neighboring cations do not differ significantly. On the other hand, the decrease of the barriers with increasing Ba and Co content—e.g., from 0.72 eV for $Ba_{0.5}Sr_{0.5}FeO_{3-\delta}$ to 0.47 eV for $Ba_{0.5}Sr_{0.5}Co_{0.8}Fe_{0.2}O_{3-\delta}$—appears related to the energetic cost for redistributing some electron density from the migrating O to the neighboring transition metal (and thus to decrease its effective size) in the transition state.

The pO_2 dependence of k^q for BSCF as measured on dense films exhibits slopes m in $k^q \propto (pO_2)^m$ in the range of 0.54 for $SrFeO_{3-\delta}$ to 0.82 for $Ba_{0.5}Sr_{0.5}FeO_{3-\delta}$.[8] The overall pO_2 dependence results from the reaction order of adsorbed oxygen species (1 for molecular adsorbate, 1/2 for atomic O resulting from a preceding fast dissociation reaction in quasiequilibrium) and contributions from point defects involved in the rate of the *rds* such as $V_{\ddot{O}}$ or electrons. Since the exponent of the pO_2 dependence of electron and $V_{\ddot{O}}$ concentration is always negative (while its magnitude will depend on the actual material), the defect contributions will decrease the overall pO_2 dependence to values lower than the reaction orders of adsorbed oxygen (1 for molecular species, 1/2 for atomic species); therefore, values larger than 1/2 clearly indicate molecular oxygen species such as O_2^-, O_2^{2-} are involved in the *rds*.

Figure 5 shows a mechanism, which is in accordance with the experimental findings, that $V_{\ddot{O}}$ migration as well as molecular oxygen species appear in the *rds*. Chemisorption is fast on the surface while it would be slower directly into

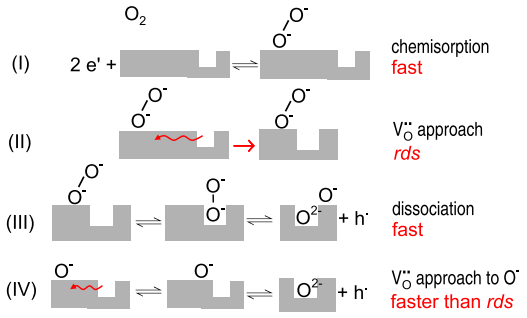


FIG. 5. Scheme of suggested reaction mechanism for BSCF perovskites.

a $V_{\ddot{O}}$ (less vacancies available as adsorption site than transition metal ions, and more strict requirements on the orientation of O_2 approaching from gas phase). After fast chemisorption (I) on the surface, the *rds* consists of the approach of an oxygen vacancy to the adsorbed O_2^{2-} (II). In analogy to the DFT results for LSM, the following dissociation (III) is expected to occur fast with negligible barrier. The approach of another $V_{\ddot{O}}$ to the remaining O_{ad}^- (IV) is faster than the *rds* due to the larger coverage with O_{ad}^-. The equilibrium exchange rate $\Re_0$ ($\propto k^q$, k^{*31}) for this proposed mechanism is

$$\Re_0 = \sqrt{\vec{R}\overleftarrow{R}} = \vec{R} \propto [O_2^{2-}][V_{\ddot{O}}]D_{V_{\ddot{O}}}$$
$$\propto K(pO_2)^1[e']^2[V_{\ddot{O}}]D_{V_{\ddot{O}}} \quad , \qquad (1)$$

where square brackets indicate concentrations, K is the mass action constant of the chemisorption, and $D_{V_{\ddot{O}}}$ represents the mobility of the approaching $V_{\ddot{O}}$. In contrast to LSM, in BSCF, the bulk $V_{\ddot{O}}$ concentration is high and the bulk migration barrier low so that the $V_{\ddot{O}}$ approach to adsorbed oxygen can occur not only by diffusion in the surface layer but also from the bulk. Thus, in contrast to LSCF, it is also plausible that rather $V_{\ddot{O}}$ migrates toward O_2^{2-} before dissociation and not vice versa. The lowering of the overall pO_2 dependence from the upper limit of $m = 1$ is mainly due to the contribution of electrons in Eq. (1) since the pO_2 as well as T-dependence of $[V_{\ddot{O}}]$ is small. This suggests that probably, the two electrons donated to the adsorbed oxygen are not transferred from $(Co,Fe)^{3+}$ species (the $(Co,Fe)^{3+}$ concentration has a comparably small pO_2 and T-dependence like $[V_{\ddot{O}}]$) but from other electronic states (e.g., $(Co,Fe)^{2+}$ originating from T- and pO_2-dependent disproportionation of Co^{3+}[46,47] and/or O deficiency when $\delta > 0.5$). Also the activation energy of k (1.4–1.6 eV for k^q of $Ba_{0.5}Sr_{0.5}Co_yFe_{1-y}O_{3-\delta}$[8]; other literature values 1–1.4 eV[42,48,49]) cannot be due to $V_{\ddot{O}}$ migration (0.5 eV) and oxygen adsorption (probably with an enthalpy close to zero) alone but has a certain contribution from the T-dependent electron concentration.

https://doi.org/10.1557/jmr.2012.186 Published online by Cambridge University Press

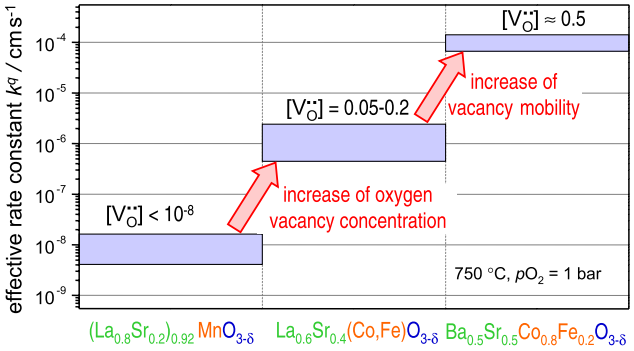


FIG. 6. Comparison of effective rate constants k^q for oxygen exchange for LSM, LSCF, and BSCF films on YSZ. Data from Refs. 7, 8, and 14. The vacancy concentration $[V_O^{\cdot\cdot}]$ is given as $V_O^{\cdot\cdot}$ per perovskite formula unit.

C. Mechanistic interpretation of the observed k–σ_{ion} correlation

Based on this mechanistic discussion in the previous section, the differences in the exchange rates between LSM, LSCF, and BSCF can largely be interpreted as shown in Fig. 6. The increase from LSM to LSCF is essentially due to the increased vacancy concentration since $V_O^{\cdot\cdot}$ are involved in the *rds*. How far the $V_O^{\cdot\cdot}$ actually migrate in the *rds* is less relevant as the vacancy mobility at a given temperature is in good approximation independent of cation composition for these perovskites.[23,39] The rate increase from LSCF to BSCF is mainly caused by the increased $V_O^{\cdot\cdot}$ mobility as the relative increase in $V_O^{\cdot\cdot}$ concentration is small.

Despite some scatter, in the double logarithmic plot of Fig. 1(b), the data points seem to follow a correlation with a slope close to 0.5 in the left part and gather between the dashed lines with slopes close to 1 and 0.5 in the right part. These limiting values of the slopes can be understood on the basis of the underlying mechanisms. The slope close to 0.5 in the left part corresponds to the correlation between k^* and D^* previously found for $(Ln,Sr)(Mn,Fe,Co)O_{3-\delta}$ perovskites.[20,50] (As the DFT results for LSM indicate a higher surface $V_O^{\cdot\cdot}$ concentration and mobility than in bulk, the LSM data should appear further right in the plot, but since k^* may be underestimated due to experimental limitations,[51] the effects on the slope may largely cancel.) For the perovskites in the left part of Fig. 1(b), the $V_O^{\cdot\cdot}$ mobility is essentially independent of cation composition.[23,39] The increase of σ_{ion} can be ascribed to the increased $V_O^{\cdot\cdot}$ concentration and thus to the oxidation enthalpy ΔH_{ox} (= -$V_O^{\cdot\cdot}$ formation enthalpy) decreasing from manganate to cobaltate perovskites.[50] Parallel to decreasing ΔH_{ox}, the oxygen chemisorption enthalpy decreases,[41] and the resulting smaller adsorbate coverages will counterbalance a part of the rate increase caused by the increased $V_O^{\cdot\cdot}$ concentration.

The mechanistic interpretation of the k^*–D^* correlation given in Ref. 50 must be updated in one point: according to the present picture, the *rds* is not the "dropping" of O_{ad}^- into a neighboring $V_O^{\cdot\cdot}$ (this was found to occur without barrier in the DFT results for LSM[10]) but the encounter of $V_O^{\cdot\cdot}$ and adsorbed oxygen. What is in common is that $V_O^{\cdot\cdot}$ are involved in the *rds*, and that the change in $V_O^{\cdot\cdot}$ concentration with changing oxidation enthalpy is the origin of the correlation. The contribution $b\Delta H_{ox}$ to the activation energy of k^*[50] corresponds to the combined (and partly compensating) effect of ΔH_{ox} on $V_O^{\cdot\cdot}$ concentration and adsorbate coverage, while $b\Delta H^{\neq}$ matches with the decreased $V_O^{\cdot\cdot}$ migration barrier in the surface layer ($0.5 \leq b \leq 0.7$, $\Delta H^{\neq}$ = $V_O^{\cdot\cdot}$ migration enthalpy). The correlation between k and the "oxygen p-band center" from DFT suggested in Ref. 52 is a largely similar finding, as the O p-band center is closely related to ΔH_{ox}. The attempt of rationalizing the trends in ΔH_{ox} in terms of *d*-electron configuration in Ref. 53 seems not really appropriate since it deals with the 2+/3+ redox couple, while the relevant couple under SOFC conditions is 3+/4+ for most materials.

A slope close to 1 as observed in the right part of Fig. 1(b) corresponds to the correlation between k^* and σ_{ion} found for $(Ba,Sr)(Fe,Co)O_{3-\delta}$.[8] Such a slope will arise from the general proportionality of k to σ_{ion} for reaction mechanisms involving $V_O^{\cdot\cdot}$ migration in the *rds*, when the increase of k is mainly due to an increase of $V_O^{\cdot\cdot}$ mobility, i.e., the enthalpy of oxidation remains approximately constant, and thus, the opposing effect of decreasing adsorbate coverage is absent.

Since electronic charge carriers appear in the chemisorption equilibria preceding the *rds*, the electronic structure (position of Fermi level) can also have some influence. On the other hand, it is expected that for most of the discussed materials, such effects are less significant than the differences in σ_{ion}, which span a range of 9 orders of magnitude.

Based on these interpretations, the question arises to what limit the surface exchange rates could further be increased. For fast exchange, (i) a high $V_O^{\cdot\cdot}$ concentration combined with (ii) chemisorption enthalpies as negative as possible and (iii) a high $V_O^{\cdot\cdot}$ mobility are desired. The first two points are to significant extent coupled to the oxidation enthalpy ΔH_{ox}, a decrease of which will increase $[V_O^{\cdot\cdot}]$ at the expense of a lower adsorbate coverage. The (molecular) adsorbate coverage might be increased by tuning parameters such as the polarizability or basicity of the cations (although to some extent, they will also be coupled to the oxidation enthalpy). With respect to $V_O^{\cdot\cdot}$ mobility (iii), BSCF appears to be already close to the maximum that can be achieved in perovskites, and the high mobility seems to be related to the Ba/Co size mismatch, which, on the other hand, facilitates unwanted transformation to hexagonal perovskite phases.[11,54,55] BSCF has further shortcomings with respect to SOFC operation (see e.g., Ref. 8). Another approach could be a combination of two phases being intimately mixed (with grain sizes smaller than in usual perovskite/electrolyte composite cathodes), one fostering oxygen adsorption and the other supplying a high vacancy concentration and mobility for the final incorporation.

https://doi.org/10.1557/jmr.2012.186 Published online by Cambridge University Press

Layered double perovskites and perovskite-related Ruddlesden–Popper phases are currently under intensive investigation. Nevertheless, in the vast majority of studies, significantly higher k values than BSCF have not been achieved so far (see e.g., Refs. 56 and 57). A particular feature of the Ruddlesden–Popper phases is that in the *ab* planes, oxygen diffusion occurs by an interstitialcy mechanism, i.e., not requiring $V_{\ddot{O}}$.[58] Interestingly, exchange rates higher than that for the single phases are reported for $(La,Sr)CoO_{3-\delta}/(La,Sr)_2CoO_{4\pm\delta}$ composites and heterostructures.[59,60] As another means for improvement, moderate tensile strain (up to few percent) has the potential to accelerate the surface reaction by the effects of increased $V_{\ddot{O}}$ concentration, $V_{\ddot{O}}$ mobility, and adsorbate coverage,[6,61] if the strain can actually be sustained and does not relax, e.g., by formation of higher-dimensional defects.

Finally, one may ask why the surface reaction on mixed conducting perovskites—in the majority of cases discussed here limited by the migration of a (surface) oxygen vacancy—is typically so slow that the subsequent bulk oxygen transport is faster even over a distance of 100 nm (i.e., involving thousands of bulk $V_{\ddot{O}}$ jumps). One major reason is that the oxygen incorporation reaction has a strongly negative entropy (loss of translational and rotational degrees of freedom) of typically $\Delta S^0 \approx -190$ J/mol K per O_2 at 1000 K. This value is estimated from ΔS^0 for oxide formation (SrO, BaO, Mn_2O_3, Fe_2O_3, Co_3O_4), and amounts to about 3/4 of the absolute entropy S^0 of gaseous O_2; ΔS^0 for oxygen incorporation in $La_{1-x}Sr_xCoO_{3-\delta}$[40] is also comparable. The respective contribution of $-T\Delta S^0 \approx$ 1.9 eV to the standard Gibbs enthalpy of reaction ΔG^0 corresponds to a factor of up to 10^{-10} appearing in the concentration of intermediate species (such as adsorbates) before the *rds*, which decreases the reaction rate accordingly (this aspect is discussed also in Ref. 62). Although chemisorption as fast preceding reaction is in quasiequilibrium, its mass action constant can affect the reaction rate by keeping the concentrations of certain intermediate species low.

IV. CONCLUSIONS

Based on the suggested reaction mechanisms, the trends in the effective rate constants for oxygen surface exchange are interpreted, which span 5 orders of magnitude in k for the mixed conducting acceptor-doped perovskites discussed here. The overall correlation with oxygen ionic conductivity can be regarded as resulting from oxygen vacancies—and in many cases, $V_{\ddot{O}}$ migration—being involved in the *rds*. This interpretation intends to give a rough outline of the fundamental properties governing surface exchange kinetics, rather than to explain all details with high quantitative precision. One has to keep in mind that the "real surfaces" can also be affected by effects from cation segregation (related, e.g., to aging phenomena) and higher-dimensional defects, which are not considered in this interpretation. While the ionic conductivity appears to be the main factor, the electronic structure can also contribute to some extent, e.g., via chemisorption equilibria preceding the *rds*. For electron-rich acceptor-doped perovskites, a high σ_{ion} (i.e., high $V_{\ddot{O}}$ concentration and/or mobility) can be utilized as a criterion in the search for SOFC cathode materials, which have to combine fast oxygen exchange kinetics with other requirements such as stability and compatibility (which may also depend on the electrolyte and operation temperature). The identification of materials with good intrinsic electrocatalytic activity is then a reliable starting point for the optimization of the actual cathode morphology, which undoubtedly also strongly affects overall SOFC performance.

ACKNOWLEDGMENTS

The authors thank G. Cristiani, B. Stuhlhofer, S. Schmid for PLD film preparation and microelectrode structuring, and G. Götz for XRD (MPI for Solid State Research, Stuttgart), J. Fleig (Technical University, Vienna), M.M. Kuklja (University of Maryland), and E. Heifets for fruitful discussions. L.W. thanks the Hans L. Merkle-Stiftung im Stifterverband für die Deutsche Wissenschaft for financial support and Y.A.M. was partly supported by EC FP7 NASA-OTM (Grant No. 228701).

REFERENCES

1. R. Merkle and J. Maier: Oxygen incorporation into Fe-doped $SrTiO_3$: Mechanistic interpretation of the surface reaction. *Phys. Chem. Chem. Phys.* **4**, 4140 (2002).
2. R. Merkle and J. Maier: The significance of defect chemistry for the rate of gas-solid reactions: Three examples. *Top. Catal.* **38**, 41 (2006).
3. W.C. Jung and H.L. Tuller: A new model describing solid oxide fuel cell cathode kinetics: Model thin film $SrTi_{1-x}Fe_xO_{3-\delta}$ mixed conducting oxides - a case study. *Adv. Energy Mat.* **1**, 1184 (2011).
4. D. Gostovic, J.R. Smith, D.P. Kundinger, K.S. Jones, and E.D. Wachsman: Three-dimensional reconstruction of porous LSCF cathodes. *Electrochem. Solid-State Lett.* **10**, B214 (2007).
5. J.R. Wilson, A.T. Duong, M. Gameiro, H-Y. Chen, K. Thornton, D.R. Mumm, and S.A. Barnett: Quantitative three-dimensional microstructure of a solid oxide fuel cell cathode. *Electrochem. Commun.* **11**, 1052 (2009).
6. G.J. la O', S.J. Ahn, E. Crumlin, Y. Orikasa, M.D. Biegalski, H.M. Christen, and Y. Shao-Horn: Catalytic activity enhancement for oxygen reduction on epitaxial perovskite thin films for solid-oxide fuel cells. *Angew. Chem. Int. Ed.* **49**, 5344 (2010).
7. F.S. Baumann, J. Fleig, G. Cristiani, B. Stuhlhofer, H-U. Habermeier, and J. Maier: Quantitative comparison of mixed conducting SOFC cathode materials by means of thin film model electrodes. *J. Electrochem. Soc.* **154**, B931 (2007).
8. L. Wang, R. Merkle, and J. Maier: Surface kinetics and mechanism of oxygen incorporation into $Ba_{1-x}Sr_xCo_yFe_{1-y}O_{3-\delta}$ SOFC microelectrodes. *J. Electrochem. Soc.* **157**, B1802 (2010).
9. L. Wang, R. Merkle, J. Maier, T. Acartürk, and U. Starke: Oxygen tracer diffusion in dense $Ba_{0.5}Sr_{0.5}Co_{0.8}Fe_{0.2}O_{3-\delta}$ films. *Appl. Phys. Lett.* **94**, 071908 (2009).

https://doi.org/10.1557/jmr.2012.186 Published online by Cambridge University Press

10. Y.A. Mastrikov, R. Merkle, E. Heifets, E.A. Kotomin, and J. Maier: Pathways for the oxygen incorporation reaction into mixed conducting perovskites: A DFT-based kinetic analysis for (La, Sr) MnO_3. *J. Phys. Chem. C* **114**, 3017 (2010).
11. R. Merkle, Y.A. Mastrikov, E.A. Kotomin, M.M. Kuklja, and J. Maier: First principles calculations of oxygen vacancy formation and migration in $Ba_{1-x}Sr_xCo_{1-y}Fe_yO_{3-\delta}$ perovskites. *J. Electrochem. Soc.* **159**, B219 (2012).
12. R.A. De Souza and M. Martin: Using $^{18}O/^{16}O$ exchange to probe an equilibrium space-charge layer at the surface of a crystalline oxide: Method and application. *Phys. Chem. Chem. Phys.* **10**, 2356 (2008).
13. J.R. Jurado, M.T. Colomer, and J.R. Frade: Impedance spectroscopy of $Sr_{0.97}Ti_{1-x}Fe_xO_{3-\delta}$ materials with moderate Fe-contents. *Solid State Ionics* **143**, 251 (2001).
14. J. Fleig, H-R. Kim, J. Jamnik, and J. Maier: Oxygen reduction kinetics of lanthanum manganite (LSM) model cathodes: Partial pressure dependence and rate-limiting steps. *Fuel Cells* **8**, 330 (2008).
15. J. Mizusaki, Y. Yonemura, H. Kamata, K. Ohyama, N. Mori, H. Takai, H. Tagawa, M. Dokiya, K. Naraya, T. Sasamoto, H. Inaba, and T. Hashimoto: Electronic conductivity, Seebeck coefficient, defect and electronic structure of nonstoichiometric $La_{1-x}Sr_xMnO_3$. *Solid State Ionics* **132**, 167 (2000).
16. J. Mizusaki, J. Tabuchi, T. Matsuura, S. Yamauchi, and K. Fueki: Electrical conductivity and Seebeck coefficient of nonstoichiometric $La_{1-x}Sr_xCoO_{3-\delta}$. *J. Electrochem. Soc.* **136**, 2082 (1989).
17. E.V. Bongio, H. Black, F.C. Raszewski, D. Edwards, C.J. McConville, and V.R.W. Amarakoon: Microstructural and high-temperature electrical characterization of $La_{1-x}Sr_xFeO_{3-\delta}$. *J. Electroceram.* **14**, 193 (2005).
18. Z. Chen, R. Ran, W. Zhou, Z. Shao, and S. Liu: Assessment of $Ba_{0.5}Sr_{0.5}Co_{1-y}Fe_yO_{3-\delta}$ (y = 0.0–1.0) for prospective application as cathode for IT-SOFCs or oxygen permeating membrane. *Electrochim. Acta* **52**, 7343 (2007).
19. V.L. Kozhevnikov, I.A. Leonidov, M.V. Patrakeev, E.B. Mitberg, and K.R. Poeppelmeier: Electrical properties of the ferrite SrFeOy at high temperatures. *J. Solid State Chem.* **158**, 320 (2001).
20. R.A. de Souza and J.A. Kilner: Oxygen transport in $La_{1-x}Sr_xMn_{1-y}Co_yO_{3\pm\delta}$ perovskites part II. Oxygen surface exchange. *Solid State Ionics* **126**, 153 (1999).
21. I.C. Fullarton, J-P. Jacobs, H.E. van Benthem, J.A. Kilner, H.H. Brongersma, P.J. Scanlon, and B.C.H. Steele: Study of oxygen ion transport in acceptor doped samarium cobalt oxide. *Ionics* **1**, 51 (1995).
22. A.V. Berenov, A. Atkinson, J.A. Kilner, E. Bucher, and W. Sitte: Oxygen tracer diffusion and surface exchange kinetics in $La_{0.6}Sr_{0.4}CoO_{3-\delta}$. *Solid State Ionics* **181**, 819 (2010).
23. T. Ishigaki, S. Yamauchi, K. Kishio, J. Mizusaki, and K. Fueki: Diffusion of oxide ion vacancies in perovskite-type oxides. *J. Solid State Chem.* **73**, 179 (1988).
24. P.M. Geffroy, J.M. Bassat, A. Vivet, S. Fourcade, T. Chartier, P. Del Gallo, and N. Richet: Oxygen semi-permeation, oxygen diffusion and surface exchange coefficient of $La_{1-x}Sr_xFe_{1-y}Ga_yO_{3-\delta}$ perovskite membranes. *J. Membr. Sci.* **354**, 6 (2010).
25. A. Rothschild, W. Menesklou, H.L. Tuller, and E. Ivers-Tiffee: Electronic structure, defect chemistry, and transport properties of $SrTi_{1-x}Fe_xO_{3-\delta}$ solid solutions. *Chem. Mater.* **18**, 3651 (2006).
26. L.M. van der Haar, M.W. den Otter, M. Morskate, H.J.M. Bouwmeester, and H. Verweij: Chemical diffusion and oxygen surface transfer of $La_{1-x}Sr_xCoO_{3-\delta}$ studied with electrical conductivity relaxation. *J. Electrochem. Soc.* **149**, J41 (2002).
27. J. Mizusaki, Y. Mima, S. Yamauchi, K. Fueki, and H. Tagawa: Nonstoichiometry of the perovskite-type oxides $La_{1-x}Sr_xCoO_{3-\delta}$. *J. Solid State Chem.* **80**, 102 (1989).
28. J. Yoo, A. Verma, S. Wang, and A.J. Jacobson: Oxygen transport kinetics in $SrFeO_{3-\delta}$, $La_{0.5}Sr_{0.5}FeO_{3-\delta}$, and $La_{0.2}Sr_{0.8}Cr_{0.2}Fe_{0.8}O_{3-\delta}$ measured by electrical conductivity relaxation. *J. Electrochem. Soc.* **152**, A497 (2005).
29. J.E. ten Elshof, M.H.R. Lankhorst, and H.J.M. Bouwmeester: Oxygen exchange and diffusion coefficients of strontium-doped lanthanum ferrites by electrical conductivity relaxation. *J. Electrochem. Soc.* **144**, 1060 (1997).
30. D. Chen and Z. Shao: Surface exchange and bulk diffusion properties of $Ba_{0.5}Sr_{0.5}Co_{0.8}Fe_{0.2}O_{3-\delta}$ mixed conductor. *Int. J. Hydrogen Energy* **36**, 6948 (2011).
31. J. Maier: On the correlation of macroscopic and microscopic rate constants in solid state chemistry. *Solid State Ionics* **112**, 197 (1998).
32. J.A. Kilner, R.A. De Souza, and I.C. Fullarton: Surface exchange of oxygen in mixed conducting perovskite oxides. *Solid State Ionics* **86**, 703 (1996).
33. M. Mosleh, M. Sogaard, and P.V. Hendriksen: Kinetics and mechanism of oxygen surface exchange on $La_{0.6}Sr_{0.4}FeO_{3-\delta}$ thin films. *J. Electrochem. Soc.* **156**, B441 (2009).
34. J. Fleig and J. Maier: The polarization of mixed conducting SOFC cathodes: Effects of surface reaction coefficient, ionic conductivity and geometry. *J. Eur. Ceram. Soc.* **24**, 1343 (2004).
35. Y.M. Choi, M.E. Lynch, M.C. Lin, and M.L. Liu: Prediction of O_2 dissociation kinetics on $LaMnO_3$-based cathode materials for solid oxide fuel cells. *J. Phys. Chem. C* **113**, 7290 (2009).
36. S. Piskunov, E. Heifets, T. Jacob, E.A. Kotomin, D.E. Ellis, and E. Spohr: Electronic structure and thermodynamic stability of $LaMnO_3$ and $La_{1-x}Sr_xMnO_3$ (001) surfaces: Ab initio calculations. *Phys. Rev. B*, **78**, 121406 (2008).
37. Y.A. Mastrikov, E. Heifets, E.A. Kotomin, and J. Maier: Atomic, electronic and thermodynamic properties of cubic and orthorhombic $LaMnO_3$ surfaces. *Surf. Sci.* **603**, 326 (2009).
38. J. Fleig, R. Merkle, and J. Maier: The $p(O_2)$ dependence of oxygen surface coverage and exchange current density of mixed conducting oxide electrodes: Model considerations. *Phys. Chem. Chem. Phys.* **9**, 2713 (2007).
39. R.A. De Souza and J.A. Kilner: Oxygen transport in $La_{1-x}Sr_xMn_{1-y}Co_yO_{3\pm\delta}$ perovskites Part I. Oxygen tracer diffusion. *Solid State Ionics* **106**, 175 (1998).
40. J. Mizusaki, M. Yoshihiro, S. Yamauchi, and K. Fueki: Nonstoichiometry and defect structure of the perovskite-type oxides $La_{1-x}Sr_xFeO_{3-\delta}$. *J. Solid State Chem.* **58**, 257 (1985).
41. Y.M. Choi, M.C. Lin, and M.L. Liu: Rational design of novel cathode materials in solid oxide fuel cells using first-principles simulations. *J. Power Sources* **195**, 1441 (2010).
42. Z. Shao and S.M. Haile: A high-performance cathode for the next generation of solid-oxide fuel cells. *Nature* **431**, 170 (2004).
43. F.S. Baumann, J. Fleig, H-U. Habermeier, and J. Maier: $Ba_{0.5}Sr_{0.5}Co_{0.8}Fe_{0.2}O_{3-\delta}$ thin film microelectrodes investigated by impedance spectroscopy. *Solid State Ionics* **177**, 3187 (2006).
44. Z.Q. Deng, W.S. Yang, W. Liu, and C.S. Chen: Relationship between transport properties and phase transformation in mixed-conducting oxides. *J. Solid State Chem.* **179**, 362 (2006).
45. S. Yakovlev, C-Y. Yoo, S. Fang, and H.J.M. Bouwmeester: Phase transformation and oxygen equilibration kinetics of pure and Zr-doped $Ba_{0.5}Sr_{0.5}Co_{0.8}Fe_{0.2}O_{3-\delta}$ perovskite oxide probed by electrical relaxation. *Appl. Phys. Lett.* **96**, 254101 (2011).
46. J-I. Jung, S.T. Misture, and D.D. Edwards: Oxygen stoichiometry, electrical conductivity, and thermopower measurements of BSCF ($Ba_{0.5}Sr_{0.5}Co_xFe_{1-x}O_{3-\delta}$, $0 \leq x \leq 0.8$) in air. *Solid State Ionics* **181**, 1287 (2010).
47. E. Bucher, W. Sitte, G.B. Caraman, V.A. Cherepanov, T.V. Aksenova, and M.V. Ananyev: Defect equilibria and partial molar properties of (La, Sr)(Co, Fe)$O_{3-\delta}$. *Solid State Ionics* **177**, 3109 (2006).
48. M. Burriel, C. Niedrig, W. Menesklou, S.F. Wagner, J. Santiso, and E. Ivers-Tiffee: BSCF epitaxial thin films: Electrical transport and oxygen surface exchange. *Solid State Ionics* **181**, 602 (2010).

https://doi.org/10.1557/jmr.2012.186 Published online by Cambridge University Press

49. H.J.M. Bouwmeester, C. Song, J. Zhu, J. Yi, M. van Sint Annaland, and B.A. Boukamp: A novel pulse isotopic exchange technique for rapid determination of the oxygen surface exchange rate of oxide ion conductors. *Phys. Chem. Chem. Phys.* **11**, 9640 (2009).
50. R. Merkle, J. Maier, and H.J.M. Bouwmeester: A linear free energy relationship for gas-solid interactions: Correlation between surface rate constant and diffusion coefficient of oxygen tracer exchange for electron-rich perovskites. *Angew. Chem. Int. Ed.* **43**, 5069 (2004).
51. R.A. De Souza: A universal empirical expression for the isotope surface exchange coefficients (k^*) of acceptor-doped perovskite and fluorite oxides. *Phys. Chem. Chem. Phys.* **8**, 890 (2006).
52. Y-L. Lee, J. Kleis, J. Rossmeisl, Y. Shao-Horn, and D. Morgan: Prediction of solid oxide fuel cell cathode activity with first-principles descriptors. *Energy Environ. Sci.* **4**, 3966 (2011).
53. M. Pavone, A.M. Ritzmann, and E.A. Carter: Quantum-mechanics-based design principles for solid oxide fuel cell cathode materials. *Energy Environ. Sci.* **4**, 4933 (2011).
54. S. Svarcova, K. Wiik, J. Tolchard, H.J.M. Bouwmeester, and T. Grande: Structural instability of cubic perovskite $Ba_xSr_{1-x}Co_{1-y}Fe_yO_{3-\delta}$. *Solid State Ionics* **178**, 1787 (2008).
55. M.M. Kuklja, Y.A. Mastrikov, B. Jansang, and E.A. Kotomin: Intrinsic defects, disordering, and structural stability of $Ba_xSr_{1-x}Co_yFe_{1-y}O_{3-\delta}$ perovskite solid solutions. *J. Phys. Chem. C* (2012, submitted).
56. A. Tarancon, S.J. Skinner, R.J. Chater, F. Hernendez-Ramirez, and J.A. Kilner: Layered perovskites as promising cathodes for intermediate temperature solid oxide fuel cells. *J. Mater. Chem.* **17**, 3175 (2007).
57. M. Burriel, G. Garcia, J. Santiso, J.A. Kilner, R.J. Chater, and S.J. Skinner: Anisotropic oxygen diffusion properties in epitaxial thin films of $La_2NiO_{4+\delta}$. *J. Mater. Chem.* **18**, 416 (2008).
58. D. Parfitt, A. Chroneos, J.A. Kilner, and R.W. Grimes: Molecular dynamics study of oxygen diffusion in $Pr_2NiO_{4+\delta}$. *Phys. Chem. Chem. Phys.* **12**, 6834 (2010).
59. M. Sase, K. Yashiro, K. Sato, J. Mizusaki, T. Kawada, N. Sakai, T. Horita, and H. Yokokawa: Enhancement of oxygen exchange at the hetero interface of (La, Sr)CoO_3/(La, Sr)$_2CoO_4$ in composite ceramics. *Solid State Ionics* **178**, 1843 (2008).
60. E.J. Crumlin, E. Mutoro, S.J. Ahn, G.J. la O', D.N. Leonard, A. Borisevich, M.D. Biegalski, H.M. Christen, and Y. Shao-Horn: Oxygen reduction kinetics enhancement on a heterostructured oxide surface for solid oxide fuel cells. *J. Phys. Chem. Lett.* **1**, 3149 (2010).
61. J.W. Han and B. Yildiz: Enhanced one dimensional mobility of oxygen on strained $LaCoO_3$(001) surface. *J. Mater. Chem.* **21**, 18983 (2011).
62. S.B. Adler, X.Y. Chen, and J.R. Wilson: Mechanisms and rate laws for oxygen exchange on mixed-conducting oxide surfaces. *J. Catal.* **245**, 91 (2007).

https://doi.org/10.1557/jmr.2012.186 Published online by Cambridge University Press